


Experimental study of coherent structures of finite-size particles in thermocapillary liquid bridges

Masakazu Gotoda, Aro Toyama, Misa Ishimura, Tomoaki Sano, Mizuki Suzuki, Toshihiro Kaneko, and Ichiro Ueno ^{*}

*Department of Mechanical Engineering, Faculty of Science and Technology,
Tokyo University of Science, Noda-shi, Chiba-ken 278-8510, Japan*



(Received 19 February 2016; published 9 September 2019)

The motion of finite-size particles in thermocapillary flow is investigated experimentally. Particular attention is paid to the unique phenomenon known as a particle accumulation structure (PAS), where particles gather in a solidlike structure in a half-zone liquid bridge. We study the correlation between the PAS and the flow field due to the hydrothermal wave instability by measuring the surface temperature and dynamic surface deformation. An image processing method is developed in order to verify the physical model of the particle behavior. The structures of the particle depletion zone, the PAS, and the toroidal core are observed clearly using long-term averaged images in the rotating frame of reference. The results of precise experiments reveal that the correlation between the PAS and the temperature field over the free surface is strongly dependent on the test fluid. Reconstruction of the PASs is achieved by applying particle tracking velocimetry. Time-series analysis of the particle position indicate that the ratio of the hydrothermal wave frequency to the turnover frequency of the particle is independent of the intensity of the thermocapillary-driven convection.

DOI: [10.1103/PhysRevFluids.4.094301](https://doi.org/10.1103/PhysRevFluids.4.094301)

I. INTRODUCTION

Investigations of the transport of momentum, heat, and mass in microsystems are very interesting and important, not only as means of furthering understanding of natural phenomena, but also for industrial applications. Examples of applications based on such research include protein crystal growth using the hanging drop method [1–5], solid and fluid segregation in industrial effluents at manufacturing plants [6,7], and the separation of deformable red blood cells within the blood [8–10]. Although it is difficult to manage microscale fluids using an external mechanical force, it would be possible to drive such fluids by the surface tension with no additional external force under specific microscale conditions. This is because the flow is dominated by the surface force under microgravity or microscale conditions but not by body forces that are dominant under normal gravity or macroscale conditions. The surface tension γ expressed as the surface force per unit length strongly depends on the inhomogeneous temperature T and/or the concentration field on the free surface. Flow driven by such a surface-tension gradient is called Marangoni convection, and temperature- and concentration-gradient-dominant flows are referred to as thermocapillary and solutocapillary convection, respectively. In the present paper, we focus on thermocapillary convection. A number of studies have been performed on thermocapillary convection using various experimental geometries such as liquid bridges [11–15], liquid layers [16–19], free liquid films

^{*}ich@rs.tus.ac.jp

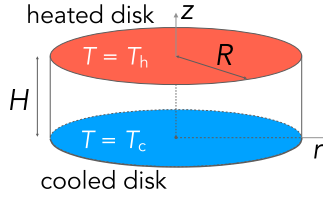


FIG. 1. Sketch of the cross-sectional view of the half-zone liquid bridge. Two horizontal disks of radius R are separated by a distance H . The top disk temperature is higher than that of the bottom disk.

[20–23], and droplets [24,25]. In particular, the so-called half-zone (HZ) liquid bridge, the top half of the floating zone [26,27], is widely employed.

In the geometry of the HZ liquid bridge (see Fig. 1), a certain amount of liquid is sustained between cylindrical coaxial rods by the surface tension of the fluid, which yields a bridge between the rod end walls. This geometry is frequently employed in fundamental investigations of thermocapillary convection because of its axially symmetric geometry. This geometry also involves a unique characteristic: Because it is closed in the azimuthal direction, modal structures in the azimuthal direction appear easily. In addition, a temperature difference ΔT can define the intensity of a thermocapillary-driven convection in terms of the designated thermal boundary conditions, because the thermocapillary effect creates a surface stress proportional to the tangential gradient of the temperature. In this geometry, one rod is cooled and maintained at a lower temperature T_c while the other is heated at a higher temperature T_h . The Marangoni number Ma describes the intensity of the thermocapillary-driven flow such that

$$Ma = \frac{|\gamma_T| \Delta T H}{\rho \nu \kappa} = Re_\gamma Pr, \quad (1)$$

where $\Delta T = T_h - T_c$ is the temperature difference between the sustaining rods; H is the height of the liquid bridge as the characteristic length of this geometry; ρ , ν , and κ are the density, kinematic viscosity, and thermal diffusivity of the test fluid, respectively; and γ_T ($=\partial\gamma/\partial T$) is the temperature coefficient of the surface tension γ . The surface tension decreases as a function of temperature for most of fluids, $\partial\gamma/\partial T < 0$. Hence, when a temperature gradient is established on the free surface, the fluid is driven by the surface tension gradient to induce convective motion toward a region of lower temperature. The Marangoni number is the product of the thermocapillary Reynolds number $Re_\gamma = |\gamma_T| \Delta T H / \rho \nu^2$ and the Prandtl number $Pr = \nu / \kappa$.

In HZ liquid bridges, it has been shown that the convection exhibits a transition from two- to three-dimensional flows if ΔT exceeds a certain threshold [12]. This threshold is referred to as the critical temperature difference ΔT_c or the critical Marangoni number Ma_c that corresponds to Ma at $\Delta T = \Delta T_c$. It has been known that the cause of the instability significantly differs depending on the value of Pr [28,29]. For a low- Pr fluid, some studies have predicted two bifurcations [30–34]. At the primary bifurcation, the hydrodynamic instability arises in the flow field, which leads the flow to three-dimensional nonaxisymmetric from two-dimensional axisymmetric. The flow remains time independent or steady at the primary instability. At the secondary bifurcation, the flow field exhibits another transition to time-dependent oscillatory convection. On the other hand, for a high- Pr fluid, it has been indicated that the flow field exhibits a primary transition from two-dimensional steady convection to three-dimensional oscillatory convection [11,12,14,35]. This transition process is governed by the hydrothermal wave (HTW) instability [36,37]. Recently, it was shown that there also exists a secondary instability even for high Pr fluids [38]. The hydrothermal wave is characterized by strong internal temperature extrema which also modify the temperature on the free surface which can be measured by contactless methods like infrared (IR) thermography [39–41]. Then a thermal wave is transmitted on the free surface, which is oriented at an angle to the end

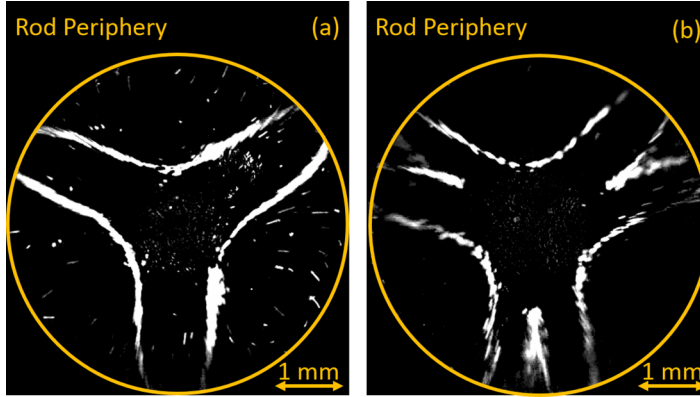


FIG. 2. Snapshots of the particle accumulation structure: (a) SL1 PAS ($Ma = 4.8 \times 10^4$) and (b) SL2 PAS ($Ma = 5.6 \times 10^4$) with particles $15 \mu\text{m}$ in diameter in the liquid bridge of $\Gamma = 0.64$ and $R = 2.5 \text{ mm}$. Images are taken from above through the transparent top rod with a constant shutter speed at $1/60 \text{ s}$.

walls of the rods that sustain the liquid bridge as a function of Pr . Modal structures with a distinct wave number in the azimuthal direction have been found to emerge beyond the critical conditions [12,14,32,42].

In the oscillatory flows, small particles converge on one-dimensional spiral closed lines rotating in the azimuthal direction, forming a solidlike structure under a limited condition in Ma . This unique phenomenon is called a particle accumulation structure (PAS) following Schwabe *et al.* [43]. Following this pioneering report, this has been investigated in significant detail by experimental, numerical, and theoretical approaches. From the experimental perspective, Tanaka *et al.* [44] indicated two major structural types, i.e., spiral-loop 1 (SL1) and spiral-loop 2 (SL2) PASs, as shown in Fig. 2. Schematic three-dimensional configurations of those PASs were reconstructed. Three-dimensional structures of SL1 [45,46] and SL2 [47] were obtained separately by tracking a single particle traveling on a PAS with three-dimensional particle tracking velocimetry (PTV).

The formation condition of the PAS has been widely examined; it has been found that a PAS is formed under specific conditions, which depend on Ma , the aspect ratio $\Gamma = H/R$, and the volume ratio V/V_0 [41,44,48–50], where R is the radius of the end surfaces of the rods to sustain the liquid bridge, V is the total volume of the liquid bridge itself, and V_0 is the volume of the straight cylinder between the end surfaces corresponding to $\pi R^2 H$. Schwabe *et al.* [48] examined extensively the effects of the size, shape, and density of the particles on the PAS formation by employing mixed fluids with NaNO_3 and CsNO_3 as the test fluids to vary the particle-fluid density ratio. Schwabe *et al.* conducted the microgravity experiment as well with the sounding rocket Maxus and concluded that “gravity is influencing the [PAS formation] by either changing the flow field or the [liquid-bridge shape] by hydrostatic deformation (and thus the flow field) but gravity may be not essential” [51]. It has been indicated that the PAS emerges in the liquid bridges for rather high Ma , which is approximately two times larger than Ma_c independently of the gravity level [41,44,48,50,51]. Recently, the formation of a PAS was also realized in another microgravity experiment conducted in the Japanese Experiment Module aboard the International Space Station (ISS) [52]. Note, however, that the PAS examined in that study was temporarily formed under transient thermal conditions in a concave liquid bridge (or $V/V_0 < 1$). It should also be noted that the formation region in terms of Ma was located just slightly above the critical conditions in that long-duration microgravity experiment with a large-size liquid bridge with $R = 15 \text{ mm}$. The shapes of the PAS also differ significantly between the microgravity experiments [52] and the ground experiments [41,43,44,48,50]. The cause of these differences is still unclear and further research is required.

The mechanism of PAS formation was examined experimentally by measuring the spatial correlation between the PAS and the temperature variation over the free surface [48]. The presented hypothesis was that the particles would gather on the free surface along a colder region due to the thermocapillary effect and then would form a PAS. It should be noted, however, that they examined a single kind of liquid (*n*-decane of $Pr = 15$) and never discussed the dependence on the Prandtl number. Subsequently, physical models to describe the PAS formation have been proposed and examined numerically [53–62]. At present, two specific models with different mechanisms for particle accumulation have been reported: the inertia dominant model [53] and the particle–free-surface interaction model [54,55]. The inertia dominant model was based on the phase locking between the flow field and the particle motion proposed by Pushkin *et al.* [53]; they suggested that a PAS would be formed by synchronization between the particle turnover motion due to the basic flow in the liquid bridge and the azimuthal convective motion due to HTW instability. Melnikov *et al.* [58] asserted that this synchronization would sometimes be destroyed, causing the particles to become detached from the PAS. The proposed phase-locking model was independently suggested by Lappa [59], who illustrated that a strong geometrical correspondence between the PAS and the isosurface of $1/2$ axial vorticity may be seen as the effect of the phase-locking mechanism under the rotation of the heated rod. The vorticity-wave model was also employed to explain the phenomenon of particle accumulations in standing-wave-type flows [63]. Using the same parameters as Pushkin *et al.* [53], Lappa [60] also evaluated the effect of g-jitters on the PAS and advocated that g-jitters parallel to the liquid-bridge axis would have a larger influence than those perpendicular to the axis. The particle–free-surface interaction model was proposed by Hofmann and Kuhlmann [54]. This model stated that the PAS would be formed through the transfer of particles that collide with the free surface to specific streamlines by considering density-matched particles. Hofmann and Kuhlmann [54] illustrated the presence of closed stream tubes in the flow in the rotating frame and that particles accumulate on these stream tubes via a finite-particle-size effect that would force particle transfer from one streamline to another. Further, Mukin and Kuhlmann [64] indicated the existence of several kinds of SL1 PASs, for example, tubular, linelike, and period-doubled PASs by varying the particle size and/or Reynolds number Re of the system. Romanò and Kuhlmann [65] conducted a series of numerical simulations on the particle motion in the thermocapillary-driven flow by applying the Maxey-Riley equation. They successfully reproduced the coherent structures, SL1 and SL2 PASs, in the HZ liquid bridge of high Pr fluids ($Pr = 28$) applying a lubrication gap near the free surface [55,56] in order to describe the particle motion in geometries with rigid or free boundaries [66]. They also indicated that the core becomes rather chaotic and less stable as Pr increases. Further, they indicated that the same accumulation is realized with and without taking account of inertia, even though the particles are heavier than the fluid. In addition to those typical PAS such as coherent structures, Kuhlmann and Muldoon [62] defined the particle depletion zone (PDZ) as a type of PAS, using the term strange PAS. Muldoon and Kuhlmann [61] illustrated that a PDZ with a triangular shape ($m = 3$) is the projection of a depleted volume with the rest of the cylindrical volume filled with particles. The volume which is occupied by particles has a certain spatial structure; only the projection gives a triangularlike shape. Recently, Romanò *et al.* [67] indicated that the particle-boundary interaction is a generic mechanism for the formation of coherent structures with finite-size particles not only in the HZ liquid bridge.

The correlation between such coherent structures and the flow fields has been discussed by applying model-flow fields. Hofmann and Kuhlmann [54] first demonstrated that there exist Kolmogorov-Arnold-Moser (KAM) tori in a certain range of the flow intensity by employing a traveling-wave-type model convection of high-Prandtl-number fluid ($Pr = 4$) in the HZ liquid bridge. The KAM tori are stationary and rigid under a certain condition in terms of the Reynolds number Re in the rotating frame of reference; the structures exhibit a rigid-body-like rotating motion with the same azimuthal velocity in the absolute coordinate system as in the PAS [56,61,64]. In addition, the correlation between the simulated particle patterns and the KAM stream tubes has been illustrated. Then an indirect comparison was made between the KAM tori in the model convection in the HZ liquid bridge and the coherent structures realized by the experiment [68]. By integrating

images of the particles observed from above in the rotating frame of reference, it was first indicated that the suspended particles were attracted to form several coherent structures, which correspond to the KAM tori predicted. Thus, the flow fields with the coherent structures are realized below the threshold for the secondary instability; the flow in the reference frame rotating with the HTW becomes time dependent [38].

In order to obtain a spatial correlation between the PAS and the flow field induced by the HTW, one has to detect any information in the phase difference among the particle trajectories, the coherent structure, and the temperature distribution over the free surface. This is one of the critical tasks for experimental investigations. An accessible feature by the experiments to obtain their spatial correlation is the dynamic surface deformation (DSD) induced by the thermocapillary-driven convection. Knowledge of the flow field and DSD has been accumulated over the past decades in addition to the investigation on the natural vibration of the liquid bridge under isothermal conditions [69]. Kuhlmann and Nienhüser [70] indicated the correlation between the HTW and the corresponding DSD through a linear stability analysis (LSA) and concluded that the dynamic surface deformation is determined by the flow at lower orders of the capillary number Ca . Hashimoto *et al.* [71] determined the correlation between the surface temperature, the DSD, the pressure, and the axial velocity of the fluid based on a numerical simulation, considering silicone oil of 2 cS ($Pr = 28$) as a test fluid. Nishino *et al.* [72] found that the amplitude of surface deformation was almost 1 μm by employing silicone oil of 5 cS ($Pr = 68$) as a test fluid through a series of experiments. Li *et al.* [73] measured the surface deformation by enlarged side-view images. Montanero *et al.* [74] performed simultaneous measurement of the temperature on the surface and DSD and found that the DSD amplitude increases as ΔT in a liquid bridge of radius $R \sim 3$ mm. Similarly, Ferrera *et al.* [75] found that the phase difference between the HTW and DSD varies as ΔT . Yasnou *et al.* [76] examined side views of a liquid bridge from two different directions and accomplished a complete reconstruction of the liquid-bridge shape. A series of microgravity experiments was conducted on the ISS with a larger-size liquid bridge of higher- Pr fluid than those in the ground experiments; Yano *et al.* [77] indicated two different patterns of DSD in the z direction depending on Γ in the oscillatory flow state. They successfully decomposed DSD into thermocapillary-driven and so-called g-jitter-driven components.

In the present study, we examine the PAS in a HZ liquid bridge obtained using nondeformable spherical particles. We focus on the variation of the coherent structures of finite-size particles as a function of the intensity of the thermocapillary effect or Ma . We illustrate the correlation between the PAS and the flow field induced by the HTW instability experimentally by way of the spatial-temporal correlation between the HTW-induced flow field and DSD.

II. EXPERIMENTAL SETUP AND PROCEDURES

The experimental apparatus is shown in Fig. 3. This figure illustrates a cross-sectional view of the apparatus. A liquid is bridged between coaxial face-to-face rods, 2.5 mm in radius. The height of the liquid bridge, or the distance between the end surfaces of the rods, is fixed at 1.6 mm throughout this research. The corresponding Γ is equal to 0.64. This is the target configuration of the liquid bridge. Basic configurations are the same as in [41,66]. The top rod is made of transparent sapphire [13]; the motion of the particles suspended by the liquid bridge is captured through the top rod. The bottom rod is made of aluminum, whose edge of the end surface is sharpened to realize a liquid bridge with a larger volume ratio than unity by pinning the contact line of the liquid bridge. The rod is coated with a black pigment to prevent light reflection and to facilitate easy observation of the suspended particles. Both rods are carefully cleaned with acetone and their sidewalls are coated with fluorine fluid to prevent test-fluid leakage. The liquid bridge is created between the two sustaining rods by supplying the test fluid through a tiny channel prepared along the centerline of the bottom rod. In order to generate thermocapillary convection, we employ a geometry in which the top and bottom rods are heated and cooled, respectively. The bottom-rod temperature T_c is kept constant at 20 °C by a cooling channel, whereas the top-rod temperature T_h is varied by an electric heater by the

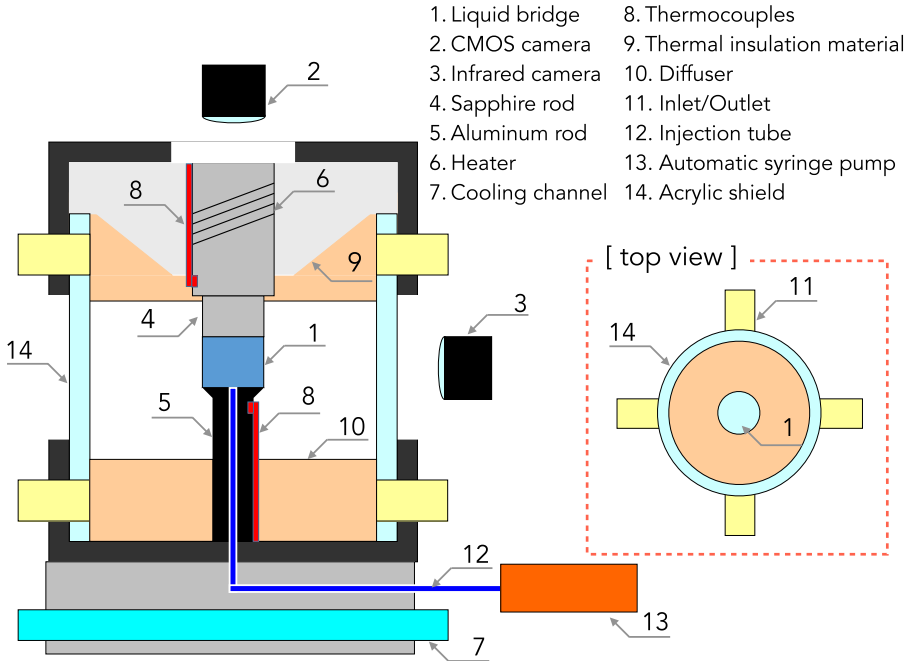


FIG. 3. Cross-sectional view of the experimental apparatus (not to scale). The liquid bridge is heated from above in this configuration. A narrow ZnSe window is placed at a portion of the external shield for the infrared camera to detect the surface temperature through the shield. The CMOS camera for the side view and the displacement sensor are omitted.

feedback temperature control system (Model 335 Cryogenic Temperature Controller, Lake Shore Cryotronics Inc., USA). Both T_c and T_h are monitored by thermocouples.

The behaviors of the tracer particles suspended by the liquid bridge are recorded from the top and the side using complementary metal-oxide semiconductor (CMOS) cameras (FASTCAM-512PCI, Photron, Inc., Japan). The frame rate of the CMOS cameras is 60 Hz and the exposure time is 1/60 s. In addition to this system for monitoring the global behavior of the PAS, a PTV technique is used to track individual particles forming the PAS in the radial-azimuthal plane. In the PTV measurements, in order to realize precise reconstruction, a high-speed camera (FASTCAM APX-RS, Photron, Inc., Japan) is used. The tracking of the particles is conducted with frame rates up to 500 Hz and 1/500-s exposure time. We also employ an IR camera (Thermography R300, NEC Avio Infrared Technologies Co., Ltd., Japan) of a 60-Hz sampling rate with a close-up lens (TVC-2100UB, NEC Avio Infrared Technologies Co., Ltd., Japan) to obtain the spatiotemporal structure of the temperature variation over the free surface caused by the HTW. In our experimental setup, the infrared camera is placed at a position $\pi/2$ away from the side-view CMOS camera. We record the images by both CMOS and infrared cameras simultaneously and we measure the fundamental frequency of the HTW, which corresponds to the rotating frequency of the PAS, from data from both the top-view CMOS camera and the IR camera. Then the synchronization between the data from the CMOS and IR cameras is achieved by delaying the phase of the data by the infrared camera based on the period that it takes to rotate the PAS 90° . A noncontact displacement sensor is placed at a position π from the infrared camera and very close to the liquid in order to measure the DSD of the liquid interface. The measuring point in the z direction is varied with an interval of 0.1 mm between the end surfaces of the top and bottom rods. We also match the phase of DSD data by considering the period of the HTW traveling between the monitoring positions. We thus realize

synchronized monitoring of the flow field, the surface temperature, and the DSD. The results on DSD and phase-matching process will be introduced in Appendix A.

To define the thermal boundary, a cylindrical tube is placed coaxially surrounding the liquid bridge as an external shield. The inner diameter of the shield and the gap between the inner wall and the liquid interface are 25 and 10 mm, respectively. A narrow ZnSe window is placed at a portion of the external shield for the infrared camera to detect the surface temperature through the shield. Note that it would be possible to add ambient gas flow around the liquid bridge with this setup by inducing forced convection inside the shield as introduced in [78]. In the present study, we add no flow inside the shield by closing inlets and outlets (component 11 in Fig. 3) installed at both ends of the shield, that is, a null forced flow of the ambient gas is employed.

Silicone oil of 2 cS in kinematic viscosity and *n*-decane are used as the test fluids, whose Pr at room temperature is 28.6 and 15, respectively. In order to keep the liquid-bridge volume at unity, the liquid is continuously injected from the center of the bottom rod so as to prevent any changes in the volume ratio due to evaporation. The flow velocity of the injected liquid, less than $5.0 \times 10^{-3} \mu\text{m/s}$, is significantly smaller than that of the Marangoni convection; for instance, Niigaki and Ueno [47] measured the velocity of the particles forming the SL2 PAS for $\text{Ma} = 4.8 \times 10^4$ to find the absolute velocity v_{ab} (in mm/s) in the range $10 \lesssim v_{\text{ab}} \lesssim 50$ and the axial velocity v_z (in mm/s) in the range $-50 \lesssim v_z \lesssim 10$. The intensity of the thermocapillary effect for the SL2 PAS is larger than the present case for the SL1 PAS, so one cannot make a direct comparison between those cases. Nevertheless, the order of the particle's velocity induced by the thermocapillary convection would be comparable. As the test particle, acrylic particles coated by gold-nickel alloy 15 and 30 μm in diameter are suspended by the liquid bridge. The particles we use are the same as those used by Toyama *et al.* [41]. These particles are suitable for flow field observations because of their solid spherical structures and high reflectivity. Importantly, we have examined that these particles do not self-adhere in silicone oil in the preliminary experiments and also in the microgravity experiments [35,79]. Note that the Stokes number St of the particles in the present geometry is of $O(10^{-5})$ – $O(10^{-4})$ under the definition [54]

$$\text{St} = \frac{\rho d_p^2}{18H^2}, \quad (2)$$

where ρ is the density ratio between the particle ρ_p and the test fluid ρ_f and d_p is the particle diameter.

III. RESULTS AND DISCUSSION

A. Structure and dynamics of particle accumulation

A typical example of the top view of coherent structures for $\text{Ma} = 2.9 \times 10^4$ is shown in Figs. 4(i) and 4(ii) for particle diameters of 15 and 30 μm , respectively. These images are obtained by accumulating over 400 inverted frames (about 7 s) in the rotating frame of reference with the fundamental frequencies of the HTW. The direction of the HTW in the laboratory frame is counterclockwise for all images. Note that these images correspond to projected images of all suspended particles observed from above. Figure 4(b) illustrates schematically major elements of the coherent structures emerging in the liquid bridge. Under this condition, the triangular shapes of the PDZ at the center of the liquid bridge are clearly formed. One can see black dots in the PDZ; these correspond to the particles deposited on the bottom-rod surface. These images in Fig. 4(b) are prepared by drawing elements *A* and *B* superimposed on the images shown in Fig. 4(a). The particles on element *A* travel in the liquid bridge toward the free surface near the heated rod shown with an arrow. The inner edges of this element correspond to the periphery of the PDZ. In the vicinity of the free surface of the liquid bridge, there exists a toroidal structure shown as element *B*, which corresponds to the toroidal core in the work of Tanaka *et al.* [44]. Note that the outer and inner edges of element *B* are drawn in a circular shape for the sake of brevity, but both edges obtained by the experiments exhibit wavy shapes as indicated in [68]. We have three regions where elements *A* and

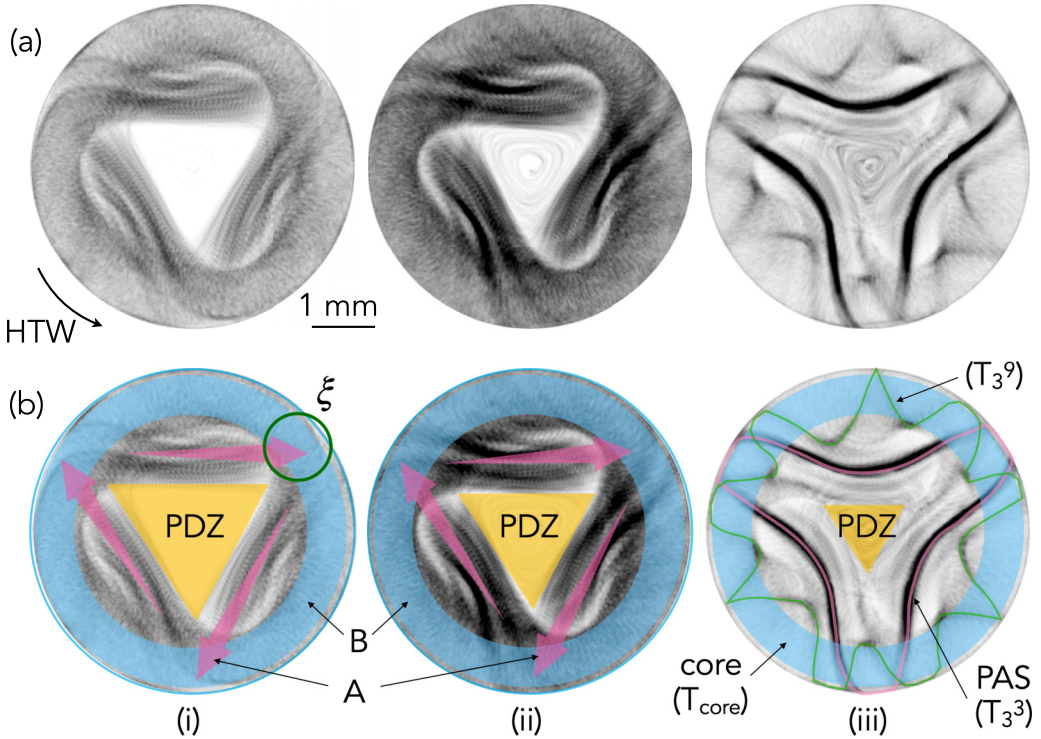


FIG. 4. Typical coherent structures in the rotating frame of reference with respect to the HTW observed from above for a Marangoni number of (i) and (ii) 2.9×10^4 and (iii) 3.8×10^4 . The diameter of suspended particles is (i) $15 \mu\text{m}$ and (ii) and (iii) $30 \mu\text{m}$. Each inverted image is obtained by averaging over 7 s (almost 10 times fundamental periods of HTW); black dots correspond to the particles and the white area corresponds to the region where no particles exist. Row (b) illustrates the major structures with multiple elements emerged in the liquid bridge schematically superimposed on the images shown in row (a). Note that the outer and inner edges of element *B* are drawn in a circular shape for the sake of brevity, but the real edges obtained by the experiments exhibit wavy shapes. The arrow for element *A* indicates the direction of the particles traveling in the bridge and its widths indicate the relative positions of the particles in the direction of the liquid-bridge height. The wider the arrows, the higher the position relative to the bottom rod. (b iii) illustrates three major coherent structures (the PAS, the core, and a structure wrapping the core) and corresponding KAM tori (T_3^3 , T_{core} , and T_3^9) following Mukin and Kuhlmann [64].

B overlap near the free surface. One of the regions is indicated by ξ in Fig. 4(bi), where the number density of the particle seems extremely small. This image also gives an impression that element *A* sneaks below element *B* and the surface flow travels from the bottom (cooled rod) to the top (heated rod); however, this is false. The fluid near the heated rod on element *A* is accelerated toward the free surface, as determined from measurements based on the images. Thus, the number density of the particle on element *A* becomes lower. Element *A* thus lies over element *B* in the region ξ when one observes from above. The correlation between elements *A* and *B* is the same as in the coherent structure in the inner part of the liquid bridge and the toroidal core as illustrated previously (see Ref. [80]). Such structures with a PDZ show good agreement with the results shown by Muldoon and Kuhlmann [61]: They indicated that there exist two separate volumes (a core and a structure wrapping around the core) in which the particles move and that the structure wrapping around the core is the precursor of a linelike PAS and is occupied by particles which have undergone at least one free-surface interaction. Element *A* in the present result corresponds to the structure that is the

precursor of the linelike PAS. In addition, it should be pointed out that element A in the region ξ exhibits twofold substructure, which was also illustrated in Fig. 20(h) in [61].

As ΔT is increased, the particles gather along closed orbits to form coherent structures in the frame of reference rotating with the HTW as shown in Fig. 4(iii). Under this condition the particles form a SL1 PAS of azimuthal wave number (or modal number) $m = 3$. Mukin and Kuhlmann [64] indicated that the particles on the chaotic streamlines move to other streamlines located inside the KAM tori following interaction with the free surface when the PAS emerges in a liquid bridge. These KAM tori are three-dimensional closed stream tubes in the liquid bridge, that is, the PAS corresponds to a torus T_3^3 and the core T_{core} . Further, a unique structure in which a particle path line winds nine times around the toroidal core is clearly observed. We believe that this structure is similar in appearance to the winding KAM torus T_3^9 proposed by Kuhlmann and co-workers [64,68]. This structure was not observed in the previous study [50], in which only 60 frames were overlapped (1 s). We consider that the exposure time in the previous study [50] was insufficient to reproduce the toroidal core structure. It should be noted that Romanò and Kuhlmann [65] did not find a KAM torus corresponding to the core of particles, but found a core of particles that was transient in a long timescale in the cylindrical liquid bridge of $\text{Pr} = 28$. In the present study, we track the particle behavior for a period of $O(1 \text{ s})$, longer than previous research [44,48]. Observation of the particle forming the core in a further longer period indicated that the toroidal core is rather hard to observe and that the particle would not be strongly attracted to the core but would migrate among coherent structures in the liquid bridge of such high Pr [81].

Figures 5(a) and 5(b) show the variations of the coherent structures obtained for particles 15 and 30 μm in diameter, respectively, in the rotating frame of reference moving with the same azimuthal rotation rate as the HTW. The values of Ma range from 3.0×10^4 to 5.2×10^4 . Note that this series of pictures is obtained from a single experimental run, i.e., the experiment is performed with the same liquid bridge and the same number of particles suspended. After monitoring the coherent structures for a certain Ma , we change Ma slightly and wait for a period of at least 900 s or 25 thermal diffusion times to fully develop the flow field and then record the particles' behaviors. The results indicate that the particles travel inside the liquid bridge except for the center region to form a particle depletion zone with a triangular shape at $\text{Ma} \sim 3.1 \times 10^4$. Some of the particles gather to exhibit dense linelike structures in an outer region of A as indicated [see Figs. 4(i) and 4(ii)]. As Ma increases, more and more particles gather on this structure (black in Fig. 5). The majority of particles have accumulated and almost perfect accumulation is realized at $\text{Ma} \sim 4.1 \times 10^4$. The degradation begins for $\text{Ma} \sim 4.9 \times 10^4$. Note that such sensitivity to ΔT was also confirmed in a previous study [50]. As seen in the frames at $\text{Ma} = 4.99 \times 10^4$ and $\text{Ma} = 5.11 \times 10^4$, the particles exhibit significant movement to escape from the PAS to a chaotic region or the toroidal core even with an $\sim 0.1 \times 10^4$ increment in Ma or 1-K increment in ΔT for 2-cS silicone oil. Although there exist morphological differences by changing the particle diameter, the scenarios of the spatial distributions of the particle trajectories are qualitatively the same. That is, elements A and B simultaneously emerge in the liquid bridge with the PDZ for lower Ma and then the PAS emerges by increasing Ma , and finally coherent structures become vague. According to the results shown in Fig. 5, it seems as if the particulate structures do not depend very much on the particle size, but more on Ma .

It should be emphasized that the SL2 PAS seldom emerges in the liquid bridge of $\Gamma = 0.64$ as seen in Fig. 5. Its range in Γ was reported by Toyama *et al.* [41]; the most favorable aspect ratio for the SL2 PAS under this condition is reported to be $\Gamma = 0.68$ (see Appendix B).

We then focus on the size of the region where the particles never penetrate. Figures 6(i) and 6(ii) show inverted images with $d_p = 15 \mu\text{m}$ in the rotating and absolute frames of reference, respectively. These images are obtained by averaging all successive frames over ten periods of oscillation. Figure 6(a) indicates the case of $\text{Ma} = 3.13 \times 10^4$ [as also shown in Fig. 5(a)] and Fig. 6(b) the case of $\text{Ma} = 4.30 \times 10^4$ [as shown in Fig. 5(b) as well]. The minimum distance from the liquid-bridge center for the linelike PAS or periodic PAS is denoted by R_{PAS} and that for the PDZ is denoted by R_{PDZ} . Note that white regions can be seen at the top and bottom right in the

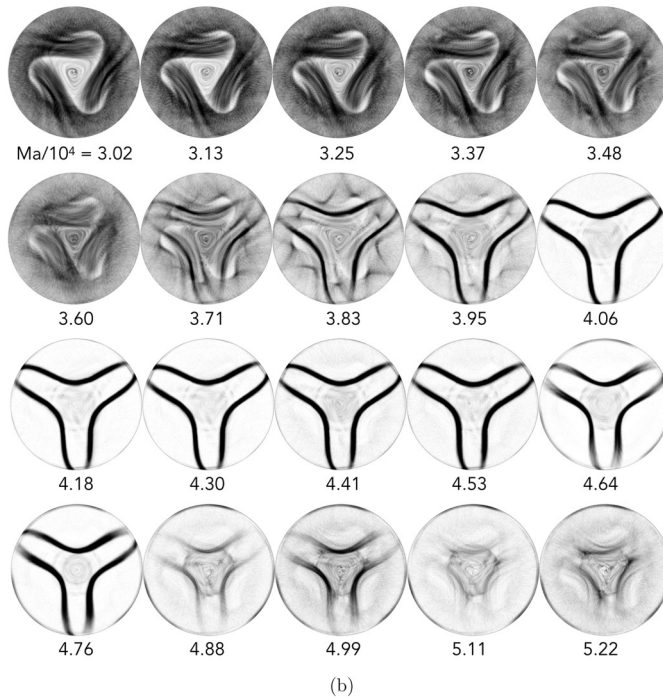
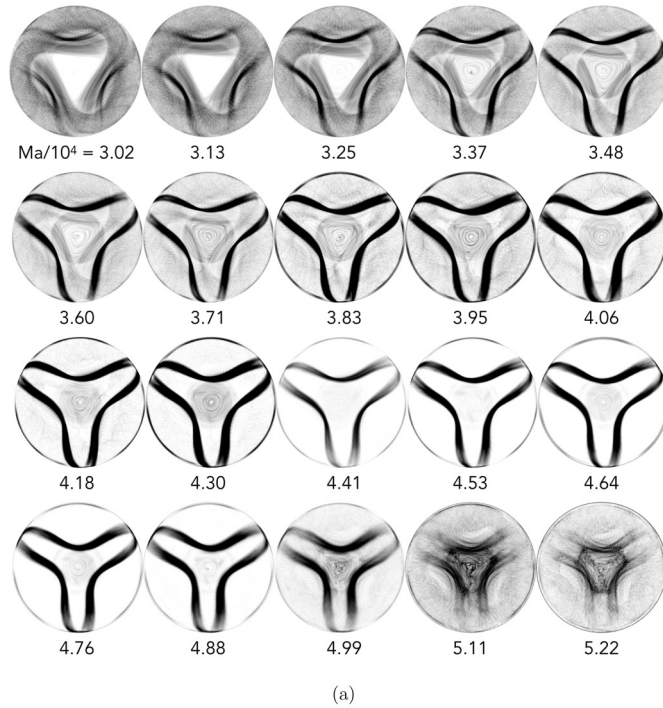


FIG. 5. Variations of coherent structures by the particles as a function of Ma for (a) $d_p = 15 \mu\text{m}$ and (b) $d_p = 30 \mu\text{m}$. Each image is obtained by averaging over 7 s (almost 10 times fundamental periods of HTW) in the rotating frame of reference with respect to the HTW. The azimuthal direction of the HTW is counterclockwise for all images.

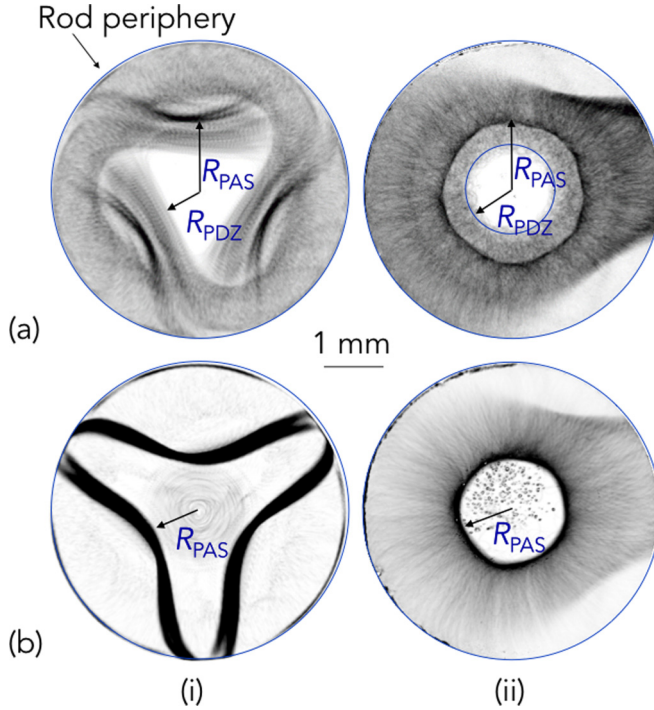


FIG. 6. Definition of the minimum distance from the liquid-bridge center for the PAS R_{PAS} and for the PDZ R_{PDZ} through top-view images obtained by averaging over 7 s (10 times fundamental periods of HTW) in (i) the rotating and (ii) the absolute frames of reference with particles $15 \mu\text{m}$ in diameter. Results are illustrated for (a) $\text{Ma} = 3.13 \times 10^4$ [as shown in Fig. 5(a)] and (b) $\text{Ma} = 4.30 \times 10^4$ [Fig. 5(b)].

images in Fig. 6(ii). These are the regions where the light from the light source never irradiates in the liquid bridge: The light is supplied to the liquid bridge through the free surface from the left in these images and one cannot avoid the refraction of the light due to the curvature of the free surface. Those regions become vague and are not apparent by integrating images for a long period in the rotating frame of reference as shown in Fig. 6(i). In the case of lower Ma to realize the PDZ [Fig. 6(a)], one finds two distinguished radii R_{PAS} and R_{PDZ} . There exist few particles inside the PDZ except the sediments, and thus we detect a sharp boundary as R_{PDZ} . There exists a denser region in component A, which corresponds the precursor of the linelike PAS. The edge of such a precursor structure results in another radius R_{PAS} . In the case of higher Ma to realize the sharp PAS [Fig. 6(b)], on the other hand, one would find a clear boundary with a radius R_{PAS} only.

Figure 7 shows variations of R_{PDZ} and R_{PAS} as a function of Ma . The very sharp boundary at R_{PAS} indicates that the region with a larger number of particles [dark in Fig. 6(ai)] is in fact distinct from the particulate structure which is characterized by R_{PDZ} . This clear separation is only visible in the laboratory frame of reference in Fig. 6(ii) and not in the rotating frame in Fig. 6(i). It is found that the particles travel far into the interior of the liquid bridge from the surface with increasing Ma . Surprisingly, larger particles reach deeper toward the center of the liquid bridge (or smaller R_{PDZ} and R_{PAS}) as seen in their variations. For the basic flow, smaller particles approach closer to the interface, so they should select the outer orbit of the basic vortex [66]. The present results, however, indicate the opposing tendency. Note that similar results on the R_{PAS} were obtained by Muldoon and Kuhlmann [61,82], although they did not notice. A possible reason is the particles are not density matched and finite size. Therefore, their trajectories deviate from streamlines as shown in Fig. 11 of [66]. We assume that R_{PDZ} and R_{PAS} are proportional to $\text{Ma}^{-n_{PDZ}}$ and $\text{Ma}^{-n_{PAS}}$, respectively. Values of

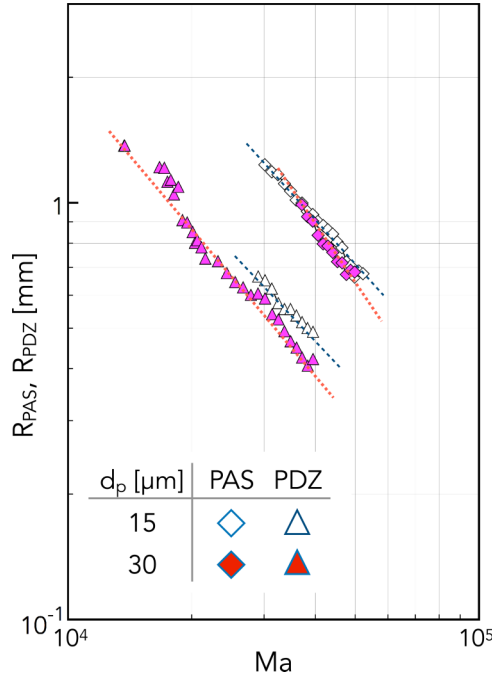


FIG. 7. Minimum radii of the PAS R_{PAS} (circles) and the PDZ R_{PDZ} (triangles) against Ma . The open and closed symbols correspond to the results with particles 15 and 30 μm in diameter, respectively.

$n_{\text{PDZ},15} \sim 1.12$, $n_{\text{PAS},15} \sim 1.13$, $n_{\text{PDZ},30} \sim 1.18$, and $n_{\text{PAS},30} \sim 1.39$ are obtained in this study, where the numbers in the subscript indicate the particle diameters in micrometers. The present results demonstrate that the power laws are dependent on the particle size and that R_{PDZ} and R_{PAS} have almost identical power values.

B. Correlation between the PAS and HTW

About a decade ago, an investigation of the correlation between a PAS and the surface temperature distribution [48] proposed that the particles gather on the free surface toward the cold spot and are finally injected into the return flow at the coldest spot on the free surface. They concluded that the particles in the liquid gathered at the cold spot on the free surface due to the surface flow induced by the thermocapillary effect; the particles accumulated at the cold spot on the interface were then aligned in a one-dimensional coherent structure. It should be pointed out that, in that study, *n*-decane was employed as the test fluid to examine the correlation between the PAS and the surface temperature, and the dependence of such results on the properties of the test fluid has not yet been discussed. In the present experiment, therefore, two different fluids are employed. First, *n*-decane is employed as the test fluid and the PAS is realized for $\text{Ma} = 3.7 \times 10^4$. This condition corresponds to the most preferable for PAS formation with the present system. This setup is used to verify the measurements against those of Schwabe *et al.* [48] and to examine the simultaneous observation with the high-speed and infrared cameras.

Figure 8(i) shows the correlation between the PAS and the temperature distribution over the free surface due to HTW instability for the *n*-decane. Images in Figs. 8(a) and 8(b) indicate inverted snapshots of the PAS observed from above and the side, respectively. The image in Fig. 8(c) shows a temperature deviation over the free surface superimposed on the side-view image [Fig. 8(b)] after the phase-matching process [25]. It should be noted that this comparison is made with the snapshots

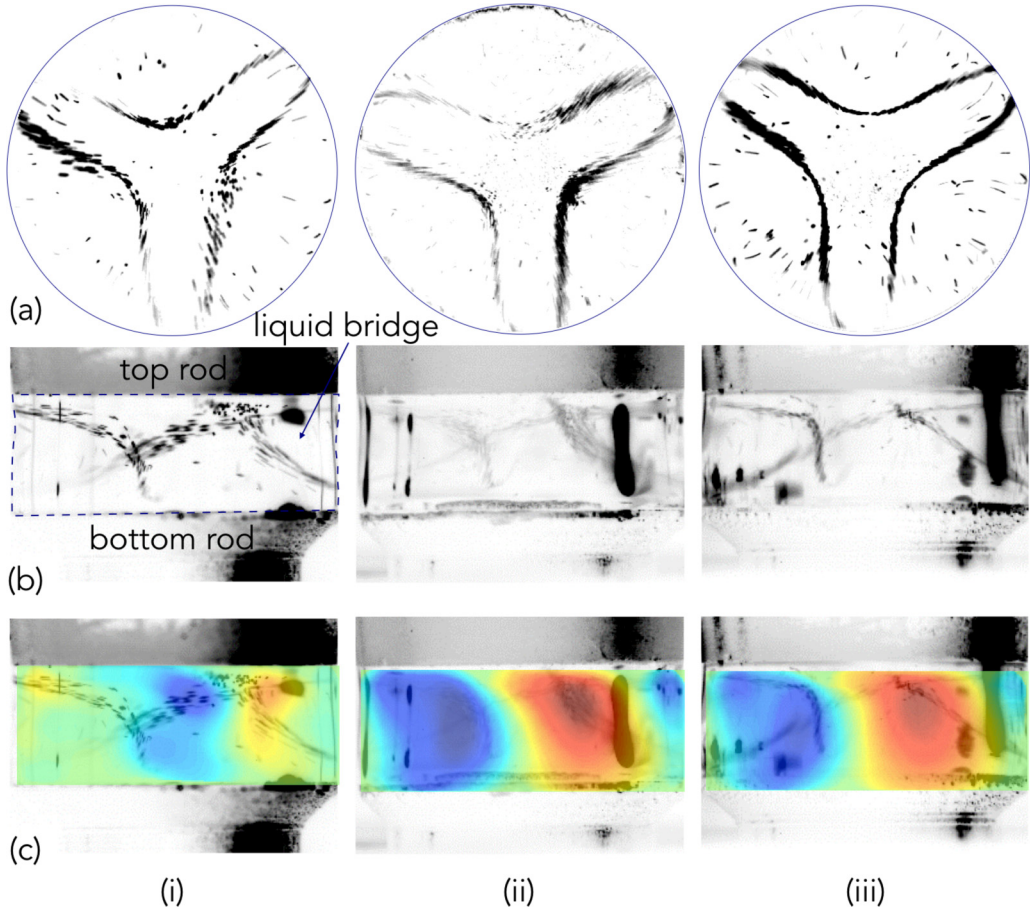


FIG. 8. Correlation between the PAS and HTW for (i) *n*-decane (at $Ma = 3.7 \times 10^4$) and (ii) and (iii) 2-cS silicone oil (at $Ma = 4.3 \times 10^4$) as test fluids from the (a) top view, (b) side view, and (c) surface temperature deviation superimposed on the side view (b). The particle diameters are (i) and (ii) $15 \mu\text{m}$ and (iii) $30 \mu\text{m}$. Red and blue indicate the hot and cold spots of the temperature deviation over the free surface, respectively. The black region on the right-hand side in each frame in (b) is the reflection of light and has nothing to do with the phenomenon concerned.

of the top and side views and the surface temperature deviation. Because *n*-decane is much more volatile than silicone oil, long-duration observation is quite difficult while keeping V/V_0 constant. Good agreement is obtained with the results of Schwabe *et al.* [48], as the particles approach the interface from the interior at the cold spot near the heated surface and then travel on the free surface almost along the colder band. The particles are then injected into the return flow at its cold spot near the cold rod. We thus confirm the present observation system to obtain a precise correlation between the particle motion and the surface temperature. We then examine this correlation with 2-cS silicone oil, in order to confirm the particle accumulation mechanism. The results indicating the correlation between the PAS and the temperature deviations due to the HTW at $Ma = 4.3 \times 10^4$ are shown in Fig. 8(ii) with the same particles as used for *n*-decane shown in Fig. 8(i). It is found that the correlations for the silicone oil and *n*-decane differ significantly; in the case of higher-Pr fluid, the particles approach the free surface in a hot spot and are injected at the neutral position into the liquid bridge. This indicates that accumulation of the fluid and particles at the cold spot on

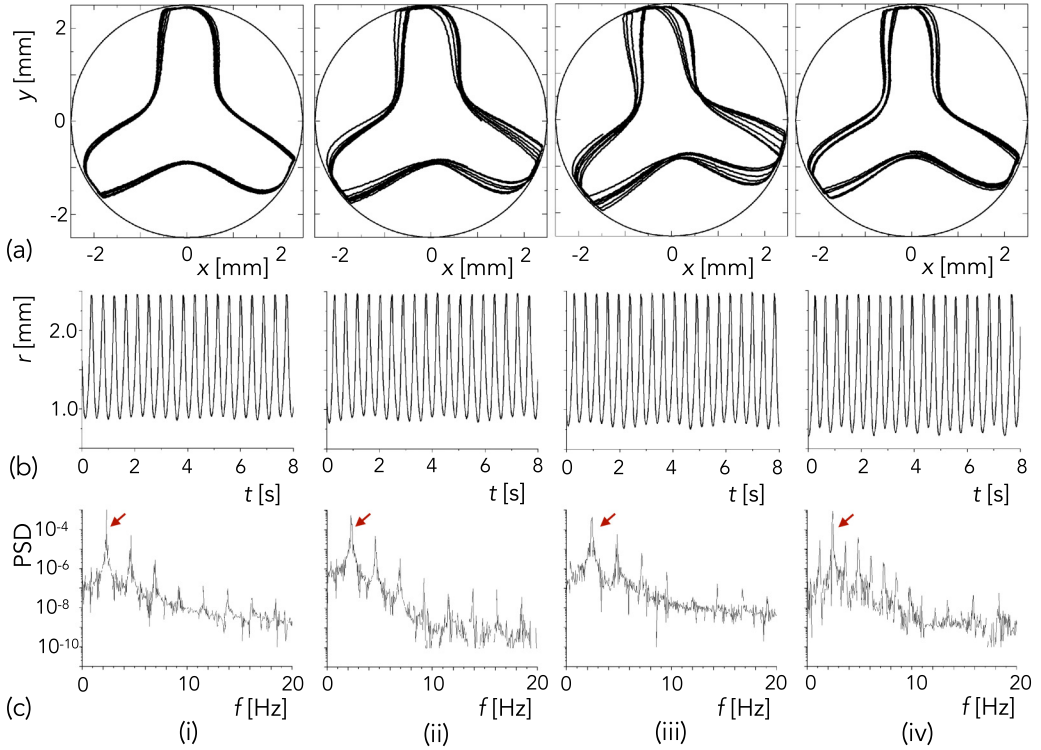


FIG. 9. (a) Reconstructed SL1 PAS configurations in the rotating frame of reference by tracking a single-particle forming the PAS, (b) time series of particle radial positions, and (c) its power spectral density (PSD) for Ma values of (i) 3.3×10^4 , (ii) 3.7×10^4 , (iii) 4.2×10^4 , and (iv) 4.6×10^4 , respectively. The particle diameter is $15 \mu\text{m}$. Arrows in row (c) indicate the fundamental frequency of the particle turnover motion f_0 .

the free surface is not an essential aspect of PAS formation. We also evaluate the effect of the size of the tracer particles. Figure 8(iii) shows the results obtained for silicone oil for the same Ma but with particles $30 \mu\text{m}$ in diameter. These findings indicate that the correlation between the thermal wave due to the HTW and PAS is rather insensitive to the particle size. In particular, we find that the particles always reach the interface at almost the same spot of the temperature deviation regardless of the particle size. A plausible explanation for this difference is that the particle motion is governed by the velocity field and not by the temperature field. The shape and phase of the temperature field with respect to the velocity field depend on Pr.

C. Harmonic and subharmonic particle accumulation

Figure 9(a) shows a single particle trajectory on the PAS for Ma = 3.3×10^4 [Fig. 9(ai)], Ma = 3.7×10^4 [Fig. 9(aii)], Ma = 4.2×10^4 [Fig. 9(aiii)], and 4.6×10^4 [Fig. 9(aiv)] in the rotating frame of reference under each condition. At Ma = 3.3×10^4 [Fig. 9(ai)], the particle trajectory is strictly periodic. For Ma = 3.7×10^4 and 4.2×10^4 [Figs. 9(aii) and 9(aiii)], PAS trajectories becomes quasiperiodic, which can also be seen from the $r(t)$ signals. At Ma = 4.6×10^4 [Fig. 9(aiv)], the particle trajectory repeats itself only after two full revolutions, indicating the presence of a subharmonic frequency $f_0/2$ in the spectrum. The most interesting feature of the particle trajectory is that there appears a closed period-doubled trajectory in the rotating frame of reference under this condition. Figure 9(b) shows the temporal variations in the particle radial

positions for the Ma concerned. The absolute minimum of the particle position in r corresponds to R_{PAS} as indicated in Fig. 6. Note that the minimum position of the particle in r is not completely constant in every period, as it exhibits periodic modulations. We also observe a specific feature at $\text{Ma} = 4.6 \times 10^4$ [Fig. 9(iv)] compared with the results at different Ma, i.e., the minimum position of the traveling particle in the radial direction exhibits a large oscillation, having alternative values of 0.7 and 0.8 mm each time as the particles penetrate to the deepest position in the liquid bridge. This behavior corresponds to the period-doubled PAS found by Mukin and Kuhlmann [64] for $\text{Pr} = 4$. Figure 9(c) shows the Fourier spectrum of the time series of the radial position of the tracked particle. The fundamental frequency of the particle turnover motion f_0 is of almost 2.3 Hz, and other harmonics occur at integral multiples of f_0 for $\text{Ma} = 3.3$ [Fig. 9(ci)], $\text{Ma} = 3.7$ [Fig. 9(cii)], and $\text{Ma} = 4.2$ [Fig. 9(ciii)]. One also finds that the modulation frequencies for the variation of R_{PAS} are 0.5 [Fig. 9(ci)], 0.3 [Fig. 9(cii)], and 0.25 Hz [Fig. 9(ciii)] from the spectra. For $\text{Ma} = 4.6 \times 10^4$ [Fig. 9(civ)], one can see a fundamental frequency $f_0 = 2.4$ Hz and its subharmonics $f_0/2 = 1.2$ Hz. This subharmonic frequency corresponds to the period-doubled trajectory of the PAS in the rotating frame. These results show that the particle motion at $\text{Ma} = 4.6 \times 10^4$ differs from those for the other three conditions. It is emphasized that Mukin and Kuhlmann [64] indicated that the period-doubled PAS appears in a strictly periodic flow. Note that the HTW is strictly periodic and not modulated under these conditions in the present experiments. Such a feature was also indicated by Toyama *et al.* [41] for Ma with SL1 and SL2 PASs and even for slightly higher Ma with no stable PASs.

We remark that Lappa [60] also observed subharmonic behaviors of the particles to form a PAS whose trajectory splits into two (referred to as D-PAS, where D indicates double). It should be noted, however, that their subharmonic response is solely due to g-jitter. In the present experiments, we believe the period-doubled structure is a result of the particle dynamics in this flow field because we do not observe any responses in the free-surface deformation as described in Appendix A.

We evaluate the frequency ratio between the particle turnover motion f_p and the HTW f_{HTW} for different Ma. Note that the fundamental frequency f_0 in Fig. 9 is directly referred to as f_p here. We find that the values of f_p/f_{HTW} become 1.58, 1.56, 1.57, and 1.59 for $\text{Ma} = 3.3 \times 10^4$, 3.7×10^4 , 4.2×10^4 , and 4.6×10^4 , respectively. The frequency ratio remains almost constant under the condition where the PAS is fully formed. That is, the ratio is independent of Ma within our experimental tolerances.

IV. CONCLUSION

The coherent structure formed by the particles suspended in a finite volume with the geometry of a half-zone liquid bridge, known as the particle accumulation structure, was investigated experimentally. The variation of the particle behaviors was finely derived as a function of the Marangoni number Ma and the particle size. We illustrated the correlation between the PAS and the thermal wave over the free surface due to the hydrothermal wave instability through the simultaneous observation system. We also indicated the frequency ratio between the particle turnover motion f_p and HTW f_{HTW} .

We illustrated the global views of the structure of the PAS. We evaluated the minimum radii of the PAS R_{PAS} and that of the particle depletion zone R_{PDZ} . We confirmed that the shapes of the PAS and PDZ are strongly dependent on Ma. The minimum radial positions R_{PAS} and R_{PDZ} as functions of Ma were found to approximately satisfy power laws. We showed the correlation between the PAS and the surface temperature distribution measured via the IR camera and indicated that their spatial correlation is dependent on the Prandtl number Pr of the test fluids. For a 2-cS silicone oil as a higher-Pr fluid, it was demonstrated that the particles on the PAS reach the hot spot on the interface near the hot-end surface and are released to the interior of the liquid bridge at the position of the neutral-temperature deviation due to the HTW. This result clearly indicated that particle accumulation at the cold spot is not crucial for PAS formation.

We examined the correlation between the HTW and the turnover motion of the particles forming a PAS. We monitored the spatiotemporal configuration of the particle on the PAS by the

two-dimensional particle tracking velocimetry technique. We then found that the frequency ratio between the particle turnover motion and HTW is almost constant and independent of Ma under the condition where the PAS is fully formed.

ACKNOWLEDGMENTS

The authors greatly appreciate financial support from the Japan Society for the Promotion of Science through a Grant-in-Aid for Scientific Research (B) (Project No. 21360101 and No. 24360078) and a Grant-in-Aid for Challenging Exploratory Research (Grant No. 16K14176). We gratefully acknowledge discussions with project members of the Japanese-European Research Experiments on Marangoni Instabilities. The authors would like to thank Akira Kawazoe for collecting some of the experimental data. We also thank Daichi Kondo and Yosuke Kowata from TUS for their helpful technical support during the experiments. I.U. acknowledges support from Tokyo University of Science through the Fund for Strategic Research Areas.

APPENDIX A: SPATIAL-TEMPORAL CORRELATION BETWEEN THE HTW AND DSD

We measure the DSD of the liquid-bridge free surface in order to illustrate the correlation among the PAS, the thermal wave over the free surface, and the DSD in the present case of $Pr = 28.6$. Two different methods are employed to measure the surface deformation: analysis of enlarged images obtained from the side-view CMOS camera and examination of the data from the noncontact displacement sensor. Figure 10 shows typical examples of DSD amplitudes at $Ma = 4.3 \times 10^4$ obtained from the enlarged side-view images. The measuring positions are at $z = 0.2$ mm (near the cooled rod) and $z = 1.4$ mm (near the heated rod) in the vertical direction from the bottom-rod surface. The dashed lines in the image indicate the instants when the tip of the PAS blades approaches the measuring point in the azimuth. This result indicates that the surface deformation has a strong dependence on the distance from the bottom rod or z position. In that case, when the tip of the PAS blade approaches the measuring point, the interface near the heated rod bulges, whereas that near the cooled rod becomes concave. The amplitude near the heated rod is slightly smaller than that near the cooled rod and these values are of submicrometer order. The tendency of the amplitude variation in the z direction is rather opposite from that obtained by Ferrera *et al.* [75] with a liquid bridge of higher Γ , slightly smaller volume ratio, and larger Pr . Note that, in the present study, we perform experiments with higher Ma values close to chaotic flow [14,44], whereas the previous research [73,74] focused on the DSD right above the flow transition points referred to as the critical Marangoni number Ma_c .

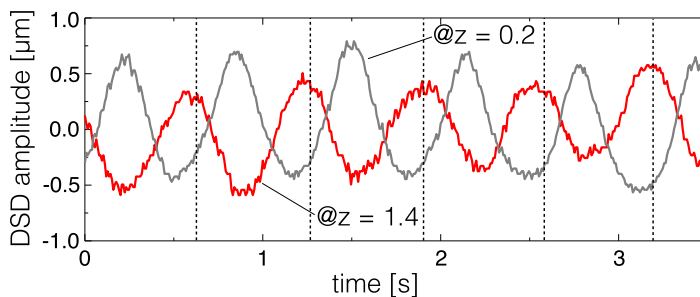


FIG. 10. Dynamic surface deformation amplitudes for $Ma = 4.3 \times 10^4$ at 0.2 and 1.4 mm from the bottom-rod surface (or $z = 0.2$ and 1.4 mm), measured based on enlarged side-view images. Dashed lines indicate the instants when the tip of the PAS blade approaches the measuring point in the azimuth.

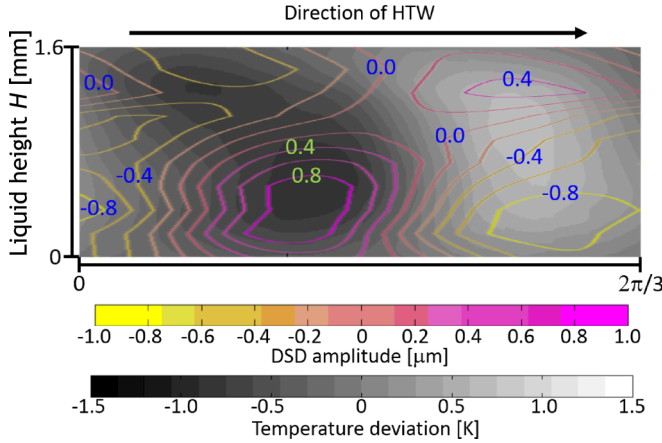


FIG. 11. Correlation between the DSD measured by the noncontact displacement sensor and temperature deviation of the thermal wave due to the HTW for $Ma = 4.3 \times 10^4$. The temperature deviation is indicated in grayscale and the DSD amplitude is indicated by the contour plot.

Figure 11 shows the correlation between the temperature deviation and DSD at $Ma = 4.3 \times 10^4$. The surface deformation is obtained using the noncontact displacement sensor data with an interval of 0.1 mm in the z direction. Contour lines are drawn by connecting data at the same value without any fitting procedures. These results exhibit the same amplitudes and the same phase shift as those obtained via different methods with the enlarged side-view images as shown in Fig. 10. In the top half of the liquid bridge, the free surface bulges or deforms outward from the liquid-bridge center in the radial direction at the hot spot, and DSD and the thermal wave due to the HTW are almost in the same phase. It is also indicated that the free surface bulges when the PAS blade approaches the interface as shown in Fig. 10. On the other hand, the phases of the DSD and the temperature deviation due to the HTW are shifted by almost π in the bottom half of the liquid bridge. In other words, the free surface bulges at the cold spot of the liquid interface. Further, the fluid may gather at the cold spot on the interface so that the liquid bulges outward. Such a correlation between the thermal wave and DSD is similar to the results obtained via an LSA for acetone ($Pr = 4.38$) under the weightlessness condition by Kuhlmann and Nienhüser [70]. In the present case for $Ma \gg Ma_c$, it can be evaluated that the thermocapillary effect is rather dominant compared to the buoyancy effect. It should be emphasized again that the Pr of the test fluid is different between Ref. [70] and the present study, so it is difficult to make a direct comparison.

APPENDIX B: PATTERN MAP IN A LIQUID BRIDGE OF $\Gamma = 0.68$

In order to reproduce a SL2 PAS in the liquid bridge, one has to focus on the flow fields in the $\Gamma = 0.68$ liquid bridge as indicated by Toyama *et al.* [41]. Figure 12 illustrates a pattern map of the particle trajectories in the rotating frame of reference with the suspended particles $5 \mu\text{m}$ [Fig. 12(a)], $10 \mu\text{m}$ [Fig. 12(b)], $15 \mu\text{m}$ [Fig. 12(c)], and $30 \mu\text{m}$ [Fig. 12(d)] in diameter. Smaller particles are attracted to exhibit a SL2 PAS for higher Ma conditions [see Figs. 12(a)–12(c)]. A SL2 PAS is hardly observed, on the contrary, if one employs larger particles such as $d_p = 30 \mu\text{m}$ [Fig. 12(d)]. Such a tendency agrees well with the previous research [44,48]. As seen in Fig. 12(d) for $Ma = 5.8 \times 10^4$, the trajectories themselves become vague and one cannot detect concrete structures. It is found that the particles follow to exhibit coherent structures for a short period, but they often change their trajectories into a central region of the liquid bridge and fall down on the bottom surface under this condition. This is why there exist no sharp structures in the whole liquid bridge.

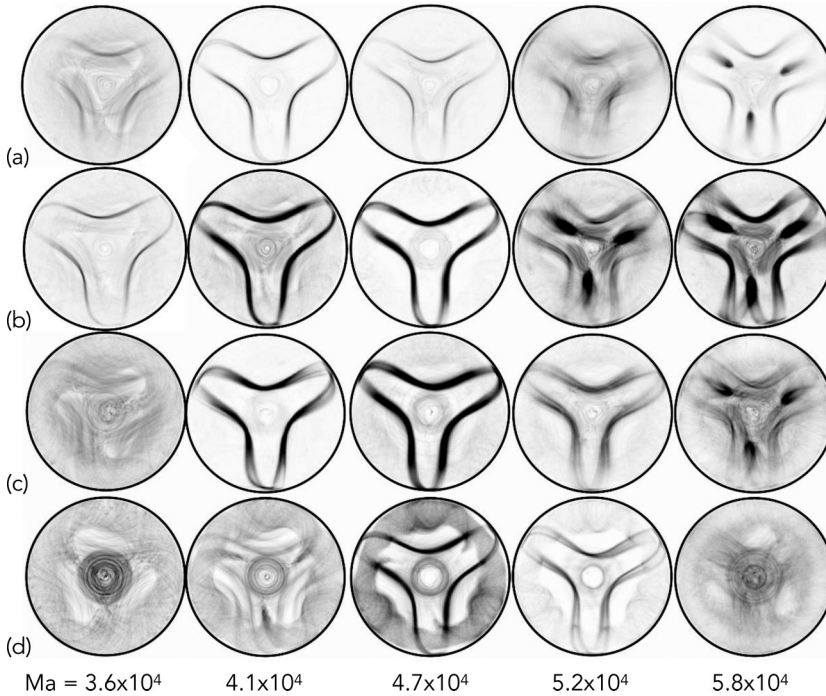


FIG. 12. Map of typical patterns by suspended particles inside a liquid bridge of $\Gamma = 0.68$ against particle size d_p and Ma . Results are shown for (a) $d_p = 5 \mu\text{m}$, (b) $d_p = 10 \mu\text{m}$, (c) $d_p = 15 \mu\text{m}$, and (d) $d_p = 30 \mu\text{m}$. Each image is obtained by accumulating 625 inverted frames (for 5 s) in the rotating frame of reference against the fundamental frequency of the HTW under each condition. The direction of the HTW in the laboratory frame is counterclockwise for all images.

-
- [1] V. Mikol, J.-L. Rodeau, and R. Giegé, Experimental determination of water equilibration rates in the hanging drop method of protein crystallization, *Anal. Biochem.* **186**, 332 (1990).
- [2] K. Provost and M.-C. Robert, Application of gel growth to hanging drop technique, *J. Cryst. Growth* **110**, 258 (1991).
- [3] J. Jancarik and S.-H. Kim, Sparse matrix sampling: A screening method for crystallization of proteins, *J. Appl. Crystallogr.* **24**, 409 (1991).
- [4] J. Day and A. McPherson, Macromolecular crystal growth experiments on international microgravity laboratory-1, *Protein Sci.* **1**, 1254 (1992).
- [5] S. Koszelak, J. Day, C. Leja, R. Cudney, and A. McPherson, Protein and virus crystal growth on international microgravity laboratory-2, *Biophys. J.* **69**, 13 (1995).
- [6] G. S. Mittal, Treatment of wastewater from abattoirs before land application—A review, *Bioresour. Technol.* **97**, 1119 (2006).
- [7] M. C. Monte, E. Fuente, A. Blanco, and C. Negro, Waste management from pulp and paper production in the European Union, *Waste Manage.* **29**, 293 (2009).
- [8] C. Sun, C. Migliorini, and L. L. Munn, Red blood cells initiate leukocyte rolling in postcapillary expansions: A lattice Boltzmann analysis, *Biophys. J.* **85**, 208 (2003).
- [9] J. P. Beech, S. H. Holm, K. Adolfsson, and J. O. Tegenfeldt, Sorting cells by size, shape and deformability, *Lab Chip* **12**, 1048 (2012).

- [10] T.-R. Lee, M. Choi, A. M. Kapacz, S.-H. Yun, W. K. Liu, and P. Decuzzi, On the near-wall accumulation of injectable particles in the microcirculation: Smaller is not better, *Sci. Rep.* **3**, 2079 (2013).
- [11] C.-H. Chun and W. Wuest, Experiments on the transition from the steady to the oscillatory Marangoni-convection of a floating zone under reduced gravity effect, *Acta Astronaut.* **6**, 1073 (1979).
- [12] F. Preisser, D. Schwabe, and A. Scharmann, Steady and oscillatory thermocapillary convection in liquid columns with free cylindrical surface, *J. Fluid Mech.* **126**, 545 (1983).
- [13] A. Hirata, S. Nishizawa, and M. Sakurai, Experimental results of oscillatory Marangoni convection in a liquid bridge under normal gravity, *J. Jpn. Soc. Microgravity Appl.* **14**, 122 (1997).
- [14] I. Ueno, S. Tanaka, and H. Kawamura, Oscillatory and chaotic thermocapillary convection in a half-zone liquid bridge, *Phys. Fluids* **15**, 408 (2003).
- [15] M. Irikura, Y. Arakawa, I. Ueno, and H. Kawamura, Effect of ambient fluid flow upon onset of oscillatory thermocapillary convection in half-zone liquid bridge, *Microgravity Sci. Technol.* **16**, 176 (2005).
- [16] J. F. Mercier and C. Normand, Buoyant-thermocapillary instabilities of differentially heated liquid layers, *Phys. Fluids* **8**, 1433 (1996).
- [17] R. J. Riley and G. P. Neitzel, Instability of thermocapillary-buoyancy convection in shallow layers. Part 1. Characterization of steady and oscillatory instabilities, *J. Fluid Mech.* **359**, 143 (1998).
- [18] N. Garnier and A. Chiffaudel, Nonlinear Transition to a Global Mode For Traveling-Wave Instability in a Finite Box, *Phys. Rev. Lett.* **86**, 75 (2001).
- [19] H. Kawamura, E. Tagaya, and Y. Hoshino, A consideration on the relation between the oscillatory thermocapillary flow in a liquid bridge and the hydrothermal wave in a thin liquid layer, *Int. J. Heat Mass Transf.* **50**, 1263 (2007).
- [20] I. Ueno and T. Torii, Thermocapillary-driven flow in a thin liquid film sustained in a rectangular hole with temperature gradient, *Acta Astronaut.* **66**, 1017 (2010).
- [21] B. Messmer, T. Lemee, K. Ikebukuro, I. Ueno, and R. Narayanan, Confined thermo-capillary flows in a double free-surface film with small Marangoni numbers, *Int. J. Heat Mass Transf.* **78**, 1060 (2014).
- [22] L. Fei, K. Ikebukuro, T. Katsuta, T. Kaneko, I. Ueno, and D. R. Pettit, Effect of static deformation on basic flow patterns in thermocapillary-driven free liquid film, *Microgravity Sci. Technol.* **29**, 29 (2017).
- [23] T. Watanabe, Y. Kowata, and I. Ueno, Flow transition and hydrothermal wave instability of thermocapillary-driven flow in a free rectangular liquid film, *Int. J. Heat Mass Transf.* **116**, 635 (2018).
- [24] I. Ueno, A. Miyauchi, and A. Kawamoto, Proceedings of the 12th International Symposium on Flow Visualization, Göttingen, 2006 (unpublished), paper no. 211.
- [25] T. Takakusagi and I. Ueno, Flow patterns induced by thermocapillary effect and resultant structures of suspended particles in a hanging droplet, *Langmuir* **33**, 13197 (2017).
- [26] A. Eyer, H. Leiste, and R. Nitsche, Floating zone growth of silicon under microgravity in a sounding rocket, *J. Cryst. Growth* **71**, 173 (1985).
- [27] A. Cröll, W. Müller, and R. Nitsche, Floating-zone growth of surface-coated silicon under microgravity, *J. Cryst. Growth* **79**, 65 (1986).
- [28] M. Wanschura, V. M. Shevtsova, H. C. Kuhlmann, and H. J. Rath, Convective instability mechanisms in thermocapillary liquid bridges, *Phys. Fluids* **7**, 912 (1995).
- [29] K. Fujimura, Linear and weakly nonlinear stability of Marangoni convection in a liquid bridge, *J. Phys. Soc. Jpn.* **82**, 074401 (2013).
- [30] R. Rupp, G. Müller, and G. Neumann, Three-dimensional time dependent modeling of the Marangoni convection in zone melting configurations for GaAs, *J. Cryst. Growth* **97**, 34 (1989).
- [31] M. Levenstam and G. Amberg, Hydrodynamical instabilities of thermocapillary flow in a half-zone, *J. Fluid Mech.* **297**, 357 (1995).
- [32] J. Leyboldt, H. C. Kuhlmann, and H. J. Rath, Three-dimensional numerical simulation of thermocapillary flows in cylindrical liquid bridges, *J. Fluid Mech.* **414**, 285 (2000).
- [33] S. Matsumoto, H. Hayashida, A. Komiya, H. Natsui, and S. Yoda, Experimental study of thermocapillary flow in the half-zone liquid bridge of low Prandtl number fluid, Annual Report of Marangoni Convection Modeling Research, NASA Report No. NASA-TMR-030004E, 2003, pp. 157–184.
- [34] K. Motegi, K. Fujimura, and I. Ueno, Floquet analysis of spatially periodic thermocapillary convection in a low-Prandtl-number liquid bridge, *Phys. Fluids* **29**, 074104 (2017).

- [35] T. Yano, K. Nishino, H. Kawamura, I. Ueno, and S. Matsumoto, Instability and associated roll structure of Marangoni convection in high Prandtl number liquid bridge with large aspect ratio, *Phys. Fluids* **27**, 024108 (2015).
- [36] M. K. Smith and S. H. Davis, Instabilities of dynamic thermocapillary liquid layers. Part 1. Convective instabilities, *J. Fluid Mech.* **132**, 119 (1983).
- [37] J.-J. Xu and S. H. Davis, Convective thermocapillary instabilities in liquid bridges, *Phys. Fluids* **27**, 1102 (1984).
- [38] T. Ogasawara, K. Motegi, T. Hori, and I. Ueno, Secondary instability induced by thermocapillary effect in half-zone liquid bridge of high Prandtl number fluid, *Mech. Eng. Lett.* **5**, 1900014 (2019).
- [39] H. Kawamura, K. Nishino, S. Matsumoto, and I. Ueno, Report on microgravity experiments of Marangoni convection aboard International Space Station, *J. Heat Transf.* **134**, 031005 (2012).
- [40] I. Ueno, H. Kawasaki, T. Watanabe, K. Motegi, and T. Kaneko, *Proceedings of the 15th International Heat Transfer Conference, Kyoto, 2014* (Begell House, Danbury, 2014).
- [41] A. Toyama, M. Gotoda, T. Kaneko, and I. Ueno, Existence conditions and formation process of second type of spiral loop particle accumulation structure (SL-2 PAS) in half-zone liquid bridge, *Microgravity Sci. Technol.* **29**, 263 (2017).
- [42] R. Velten, D. Schwabe, and A. Scharmann, The periodic instability of thermocapillary convection in cylindrical liquid bridges, *Phys. Fluids A* **3**, 267 (1991).
- [43] D. Schwabe, P. Hintz, and S. Frank, New features of thermocapillary convection in floating zones revealed by tracer particle accumulation structure (PAS), *Microgravity Sci. Technol.* **9**, 163 (1996).
- [44] S. Tanaka, H. Kawamura, I. Ueno, and D. Schwabe, Flow structure and dynamic particle accumulation in thermocapillary convection in a liquid bridge, *Phys. Fluids* **18**, 067103 (2006).
- [45] I. Ueno, Y. Abe, K. Noguchi, and H. Kawamura, Dynamic particle accumulation structure (PAS) in half-zone liquid bridge—Reconstruction of particle motion by 3-D PTV, *Adv. Space Res.* **41**, 2145 (2008).
- [46] Y. Abe, I. Ueno, and H. Kawamura, Dynamic particle accumulation structure due to thermocapillary effect in noncylindrical half-zone liquid bridge, *Ann. N.Y. Acad. Sci.* **1161**, 240 (2009).
- [47] Y. Niigaki and I. Ueno, Formation of particle accumulation structure (PAS) in half-zone liquid bridge under an effect of thermo-fluid flow of ambient gas, *Trans. Jpn. Soc. Aeronaut. Space Sci. Aerosp. Technol. Japan* **10**, Ph_33 (2012).
- [48] D. Schwabe, A. I. Mizev, M. Udhayasankar, and S. Tanaka, Formation of dynamic particle accumulation structures in oscillatory thermocapillary flow in liquid bridges, *Phys. Fluids* **19**, 072102 (2007).
- [49] T. Watanabe, D. Melnikof, T. Matsugase, V. Shevtsova, and I. Ueno, The stability of a thermocapillary-buoyant flow in a liquid bridge with heat transfer through the interface, *Microgravity Sci. Technol.* **26**, 17 (2014).
- [50] M. Gotoda, T. Sano, T. Kaneko, and I. Ueno, Evaluation of existence region and formation time of particle accumulation structure (PAS) in half-zone liquid bridge, *Eur. Phys. J. Spec. Top.* **224**, 299 (2015).
- [51] D. Schwabe, A. Mizev, S. Tanaka, and H. Kawamura, Particle accumulation structures in time-dependent thermocapillary flow in a liquid bridge under microgravity, *Microgravity Sci. Technol.* **18**, 117 (2006).
- [52] S. Matsumoto, K. Nishino, I. Ueno, T. Yano, and H. Kawamura, Marangoni experiment in space, *Int. J. Microgravity Sci. Appl.* **31**, S51 (2014).
- [53] D. O. Pushkin, D. E. Melnikov, and V. M. Shevtsova, Ordering of Small Particles in One-Dimensional Coherent Structures by Time-Periodic Flows, *Phys. Rev. Lett.* **106**, 234501 (2011).
- [54] E. Hofmann and H. C. Kuhlmann, Particle accumulation on periodic orbits by repeated free surface collisions, *Phys. Fluids* **23**, 072106 (2011).
- [55] H. C. Kuhlmann and E. Hofmann, The mechanics of particle accumulation structures in thermocapillary flows, *Eur. Phys. J. Spec. Top.* **192**, 3 (2011).
- [56] H. C. Kuhlmann and F. H. Muldoon, Particle-accumulation structures in periodic free-surface flows: Inertia versus surface collisions, *Phys. Rev. E* **85**, 046310 (2012).

- [57] H. C. Kuhlmann and F. H. Muldoon, Understanding particle accumulation structures (PAS) in thermocapillary liquid bridges, *Int. J. Microgravity Sci. Appl.* **29**, 64 (2012).
- [58] D. E. Melnikov, D. O. Pushkin, and V. M. Shevtsova, Synchronization of finite-size particles by a traveling wave in a cylindrical flow, *Phys. Fluids* **25**, 092108 (2013).
- [59] M. Lappa, Assessment of the role of axial vorticity in the formation of particle accumulation structures in supercritical Marangoni and hybrid thermocapillary-rotation-driven flows, *Phys. Fluids* **25**, 012101 (2013).
- [60] M. Lappa, On the variety of particle accumulation structures under the effect of g-jitters, *J. Fluid Mech.* **726**, 160 (2013).
- [61] F. H. Muldoon and H. C. Kuhlmann, Coherent particulate structures by boundary interaction of small particles in confined periodic flows, *Physica D* **253**, 40 (2013).
- [62] H. C. Kuhlmann and F. H. Muldoon, On the different manifestations of particle accumulation structures (PAS) in thermocapillary flows, *Eur. Phys. J. Spec. Top.* **219**, 59 (2013).
- [63] M. Lappa, Stationary solid particle attractors in standing waves, *Phys. Fluids* **26**, 013305 (2014).
- [64] R. V. Mukin and H. C. Kuhlmann, Topology of hydrothermal waves in liquid bridges and dissipative structures of transported particles, *Phys. Rev. E* **88**, 053016 (2013).
- [65] F. Romanò and H. C. Kuhlmann, Finite-size Lagrangian coherent structures in thermocapillary liquid bridges, *Phys. Rev. Fluids* **3**, 094302 (2018).
- [66] F. Romanò, H. C. Kuhlmann, M. Ishimura, and I. Ueno, Limit cycles for the motion of finite-size particles in axisymmetric thermocapillary flows in liquid bridges, *Phys. Fluids* **29**, 093303 (2017).
- [67] F. Romanò, H. Wu, and H. C. Kuhlmann, A generic mechanism for finite-size coherent particle structures, *Int. J. Multiphase Flow* **111**, 42 (2019).
- [68] H. C. Kuhlmann, R. V. Mukin, T. Sano, and I. Ueno, Structure and dynamics of particle-accumulation in thermocapillary liquid bridges, *Fluid Dyn. Res.* **46**, 041421 (2014).
- [69] A. Sanz and J. L. Diez, Non-axisymmetric oscillations of liquid bridge, *J. Fluid Mech.* **205**, 503 (1989).
- [70] H. C. Kuhlmann and C. Nienhüser, Dynamic free-surface deformations in thermocapillary liquid bridges, *Fluid Dyn. Res.* **31**, 103 (2002).
- [71] T. Hashimoto, Y. Kosaka, I. Ueno, H. Kawamura, and S. Yoda, Numerical simulation of Marangoni convection in consideration of free surface displacement, Marangoni Convection Modeling Research, JAXA Report No. JAXA-RR-04-027E, 2005, pp. 49–75.
- [72] K. Nishino, X. Li, Y. Kanashima, and S. Yoda, Dynamic surface deformation of cylindrical bridge of high Prandtl number fluid in oscillatory thermocapillary convection—TSPI measurement and G-jitter effect, Marangoni Convection Modeling Research, JAXA Report No. JAXA-RR-04-027E, 2005, pp. 25–48.
- [73] X. Li, K. Nishino, and S. Yoda, Temporal speckle pattern interferometry for measuring micron-order surface motion of a liquid bridge, *Meas. Sci. Technol.* **15**, 2284 (2004).
- [74] J.-M. Montanero, C. Ferrera, and V. M. Shevtsova, Experimental study of the free surface deformation due to thermal convection in liquid bridges, *Exp. Fluids* **45**, 1087 (2008).
- [75] C. Ferrera, J.-M. Montanero, A. Mialdun, V. M. Shevtsova, and M. G. Cabezas, A new experimental technique for measuring the dynamical free surface deformation in liquid bridges due to thermal convection, *Meas. Sci. Technol.* **19**, 015410 (2008).
- [76] V. Yasnou, A. Mialdun, and V. M. Shevtsova, Preparation of JEREMI experiment: Development of the ground based prototype, *Microgravity Sci. Technol.* **24**, 411 (2012).
- [77] T. Yano, K. Nishino, S. Matsumoto, I. Ueno, A. Komiya, Y. Kamotani, and N. Imaishi, Report on microgravity experiments of dynamic surface deformation effects on Marangoni instability in high-Prandtl-number liquid bridges, *Microgravity Sci. Technol.* **30**, 599 (2018).
- [78] I. Ueno, A. Kawazoe, and H. Enomoto, Effect of ambient-gas forced flow on oscillatory thermocapillary convection of half-zone liquid bridge, *Fluid Dyn. Mater. Process.* **6**, 99 (2010).
- [79] K. Nishino, T. Yano, H. Kawamura, S. Matsumoto, I. Ueno, and M. K. Ermakov, Instability of thermocapillary convection in long liquid bridges of high Prandtl number fluids in microgravity, *J. Cryst. Growth* **420**, 57 (2015).
- [80] M. Nishimura, I. Ueno, K. Nishino, and H. Kawamura, 3D PTV measurement of oscillatory thermocapillary convection in half-zone liquid bridge, *Exp. Fluids* **38**, 285 (2005).

- [81] K. Yamaguchi, T. Hori, and I. Ueno, Long-term behaviors of a single particle forming a coherent structure in thermocapillary-driven convection in half-zone liquid bridge of high Prandtl-number fluid, [Int. J. Microgravity Sci. Appl.](#) **36**, 360203 (2019).
- [82] F. H. Muldoon and H. C. Kuhlmann, Different particle-accumulation structures arising from particle-boundary interactions in a liquid bridge, [Int. J. Multiphase Flow](#) **59**, 145 (2014).